crystals

MDPI

Article

Oxidation Behavior and Oxide Transformation of a Pt-Modified Aluminide Coating at Moderate High Temperature

Yanyan Li [1,2], Shuai Li [1,2], Chao Zhang [3], Na Xu [1,*] and Zebin Bao [1,2,*]

[1] Shi-Changxu Innovation Center for Advanced Materials, Institute of Metal Research, Chinese Academy of Sciences, Wencui Road 62#, Shenyang 110016, China; yyli19s@imr.ac.cn (Y.L.); sli17s@imr.ac.cn (S.L.)
[2] School of Materials Science and Engineering, University of Science and Technology of China, Wenhua Road 72#, Shenyang 110016, China
[3] National Engineering Laboratory for Marine and Ocean Engineering Power System, No. 703 Research Institute of CSSC, Honghu Road 35#, Harbin 150078, China; delpiero321@163.com
* Correspondence: naxu@imr.ac.cn (N.X.); zbbao@imr.ac.cn (Z.B.)

Abstract: The oxidation performance of a single-phase Pt-modified aluminide coating was assessed in oxidation test at 980 °C in comparison with the single crystal superalloy. The results suggested that the Pt-modified aluminide coating exhibited superior oxidation resistance. During oxidation, the oxide scale formed on bare alloy changed constantly followed by the constitution of the multi-layer scale structure: An outer scale mainly consisted of Cr_2O_3 + $NiCr_2O_4$ + TiO_2 with scarce protection, and an internal scale mainly consisted of Al_2O_3. The thickness of the outer oxide scale increased with time, where the scale became looser and more porous. Meanwhile, the internal scale was discontinuous. Oxygen and nitrogen inwardly diffused into substrate, forming Ta_2O_5 and TiN particles. In contrast to the complex constitution of oxide scale, a uniform and continuous Al_2O_3 scale formed on Pt-modified aluminide-coated samples after oxidation at 980 °C for 1500 h, which showed no spallation and cracking. Interestingly, θ-Al_2O_3 and α-Al_2O_3 phases remained after such a long oxidation time. It is the relatively lower temperature and the presence of Pt retarded θ-α transformation. The degradation rate from β-NiAl to γ′-Ni_3Al was very slow in the coating. The various development of oxide scale on the coating and substrate was individually studied.

Keywords: Pt-modified aluminide coating; alumina scale; single crystal superalloy; microstructure; isothermal oxidation

check for updates

Citation: Li, Y.; Li, S.; Zhang, C.; Xu, N.; Bao, Z. Oxidation Behavior and Oxide Transformation of a Pt-Modified Aluminide Coating at Moderate High Temperature. *Crystals* **2021**, *11*, 972. https://doi.org/10.3390/cryst11080972

Academic Editor: David Holec

Received: 15 July 2021
Accepted: 15 August 2021
Published: 17 August 2021

Publisher's Note: MDPI stays neutral with regard to jurisdictional claims in published maps and institutional affiliations.

Copyright: © 2021 by the authors. Licensee MDPI, Basel, Switzerland. This article is an open access article distributed under the terms and conditions of the Creative Commons Attribution (CC BY) license (https://creativecommons.org/licenses/by/4.0/).

1. Introduction

Nickel-base single crystal (SX) superalloy series have been widely used as structural material in the hot-section components of aero, gas turbines, small type turbines and turboshaft engines [1,2], because of its satisfactory mechanical property (e.g., creep-resistance and rupture life) at high temperature. Albeit holding excellent mechanical property, the oxidation rate of superalloy increases significantly once the temperature exceeds 900 °C. As serving in harsh oxygen-rich environment, the high-temperature oxidation performance plays a critical role in determining the service life of SX superalloys, which depends on the formation of a dense and protective oxide scale (mainly refers to Al_2O_3 or Cr_2O_3) on the surface. A continuously complete oxide scale can effectively inhibit continued ingress of oxygen to the substrate alloy [3–5]. Upon exposure, if the critical Al/or Cr concentration required to maintain a protective oxide scale is not retained by the alloy, the alloy will quickly be failed [6]. Because the SX superalloys contain limited Al (<7 wt.%), it is essentially necessary to apply a high temperature protective coating on the surface of the alloys.

Pt-modified aluminide coatings have been proved to be satisfactory because of its superiority of resisting both high temperature oxidation and hot corrosion for protecting SX superalloys [7,8]. Amazingly, the refurbished Pt-modified aluminide coating also exhibited superior isothermal and cyclic oxidation resistance at 1100 °C [9]. Several studies [10–13]

have shown that the presence of Pt can promote uphill diffusion and selective oxidation of Al, improve the stability of alumina and decrease the oxidation rate. Pt can be acting as a 'cleanser' at the oxide scale/coating interface by restraining the formation of voids or quickly filling in the voids, which enhances adhesion of alumina scale and lowers the tendency of scale spallation. A conventional preparation process of a Pt-modified aluminide coating consists of a pre-deposition of a Pt layer and a successive aluminization using either pack cementation, slurry, composite electrodeposition techniques, 'above-pack' or chemical vapor deposition (CVD) methods. The high-temperature-low-activity (HTLA) above-pack treatment can produce the exclusive β-(Ni,Pt)Al phase as the CVD technique does.

In this paper, a single-phase Pt-modified aluminide coating was prepared on a first-generation SX superalloy by Pt-electrodeposition and subsequent aluminization using the 'above-pack' treatment. As the servicing temperature of the electric gas turbine or small type turbine engine and turboshaft engine is generally 950–1000 °C, we investigate the isothermal oxidation performance of the Pt-modified aluminide coatings at 980 °C in static air, in comparison with the bare SX superalloy. The purpose of carrying out this study is to observe microstructural evolution of oxide scale during long-term oxidation and to discuss the various oxidation behavior of the coating and the SX substrate.

2. Materials and Methods

A Ni-base single crystal superalloy with nominal composition of Ni-12Cr-9Co-3.7W-1.9Mo-5Ta-3.6Al-4Ti (wt. %) was used as the substrate. Cylindrical samples with dimensions of Φ17 × 2 mm were cut from the SX superalloy rod using a wire cutting machine (EDM, DK7720, Founder CNC Machine Tool Co., Jiangsu, China). The samples were ground up to 400 mesh SiC sandpaper, and then sand-blasted with 300 mesh alumina grits at 0.3 MPa. Before Pt electroplating, the samples were degreased by two-step processing: (1) Boiling in NaOH solution (10 g/L) for 10 min; (2) ultrasonic cleaning in acetone and ethanol for 20 mi, respectively. A basic Pt-plating solution was utilized to deposit the Pt layer with a thickness of ~5 μm. The details of electroplating parameters can be referred to our recent publication [14]. After that, the samples with Pt layer were annealed in a vacuum tube furnace at 1×10^{-3} Pa at 1050 °C for 1 h. Eventually, an aluminizing treatment was performed using the above-pack manner at 1060 °C for 5 h to obtain the single-phase (Ni,Pt)Al coating. The heating rate was about 10 °C/min. The aluminizing powder mixture was composed of FeAl powder (96 wt. %) and NH_4Cl (4 wt. %) activator. The surface and cross-sectional morphologies of the single-phase (Ni,Pt)Al coating prepared on SX substrates are shown in Figure 1. A typical morphology of the outwardly-grown coating that consists of (Ni,Pt)Al outer zone and underlying inter-diffusion zone (IDZ) is observed. Pt is present in the solid solution in β-NiAl, as the crystal lattice of NiAl has been enlarged to a greater extent due to the effect of Pt [1,11,15].

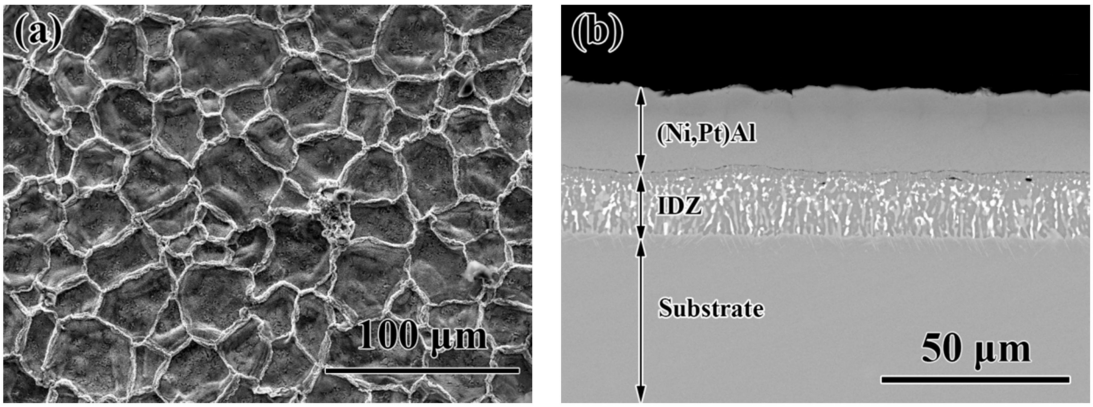

Figure 1. Surface (**a**) and cross-sectional (**b**) morphologies of as-prepared Pt-modified aluminide coating.

Isothermal oxidation test of the SX alloy samples with and without Pt-modified aluminide coating was performed in a muffle furnace at 980 °C for 1500 h in static air. The samples were taken out from the furnace after 300, 500, 1000 and 1500 h, respectively. X-ray diffraction (XRD, X'Pert, Cu Kα, PANalytical Co., Netherlands) was used to analyze the phase constitution of samples with and without (Ni,Pt)Al coating after different oxidation times. The microstructure and chemical composition of the samples was analyzed using a scanning electron microscope (SEM, Inspect F50, FEI Co., Hillsboro, Oregon) equipped with X-ray Energy Dispersive Spectroscopy (EDS, X-Max, Oxford Instruments Co., Oxford, UK). To protect oxidation products from possible spallation, the oxidized samples for cross-sectional observation were deposited a thin layer of electroless Ni-plating, then mounted in epoxy resin and polished to a mirror.

3. Results

3.1. Phase Composition

Figure 2 shows the XRD patterns of the substrate alloy after oxidation at 980 °C for 300 h, 500 h, 1000 h and 1500 h, respectively. The predominant phases on the surface after 300 h are Cr_2O_3, TiO_2 and $NiCr_2O_4$ with weak Al_2O_3. In addition, the γ/γ' matrix phase can be detected. The XRD results after oxidation for 300, 500, 1000 and 1500 h are similarly identical. When the oxidation time was extended to 1500 h, the peaks of the γ/γ' phase became weak, which is due to increase of oxide thickness (the depth of X-ray is limited).

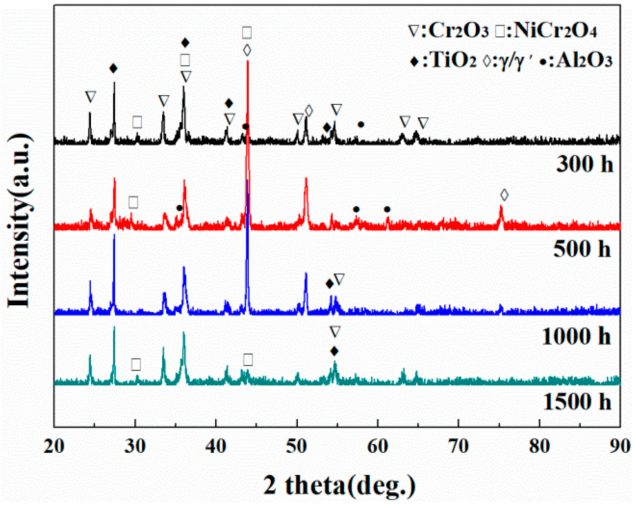

Figure 2. XRD patterns of the SX superalloy after isothermal oxidation at 980 °C for 300, 500, 1000 and 1500 h.

For the (Ni,Pt)Al coating, the XRD results (Figure 3) reveal that the oxidation product during the isothermal oxidation at 980 °C consists of exclusive Al_2O_3 and the coating phase of β-(Ni,Pt)Al can be detectable throughout the entire oxidation test. No peak of the γ/γ' phase can be identified, indicating that the (Ni,Pt)Al coating exhibited good oxidation resistance and capability of extending service life.

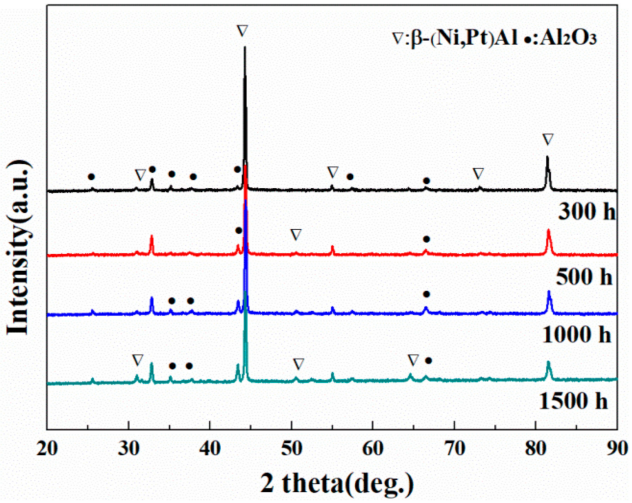

Figure 3. XRD patterns of (Ni,Pt)Al coating after isothermal oxidation at 980 °C for 300, 500, 1000 and 1500 h.

3.2. Surface Morphology

The surface morphologies of the SX superalloy substrate after isothermal oxidation at 980 °C for different times are shown in Figure 4. The average compositions of the marked regions are summarized in Table 1. After oxidation for 300 h (Figure 4a), the thick inhomogeneous oxide is clear to observe. The EDS analysis of the cauliflower-like island (Label 1) in Figure 4a shows relatively high contents of Cr and Ti. The combination of XRD and EDS results reveals that $NiCr_2O_4$, TiO_2 and Al_2O_3 are present in this region. The flat area (label 2) mainly comprises Al_2O_3, in addition to minor TiO_2, $NiCr_2O_4$ and Cr_2O_3. It can be seen from the high magnification morphology that the oxide scale in the flat area with a high Al content is dense to provide a barrier for the diffusion of oxygen. After 500 h, the surface morphology is shown in Figure 4b. The composition of both the coarse region and the flat region is not different from that in 300 h. After isothermal exposure for 1000 h, the coarse region enlarges and contains large particles (Figure 4c), which suggests that Al-concentration decreases and accordingly the concentration of Cr and Ti increases (Table 1). When oxidation prolongs to 1500 h (as shown in Figure 4d), the coarse region almost covers the entire surface of the substrate alloy that is rich in Cr and Ni, conforming to the XRD analysis. The oxide product is primarily constituted of non-protective oxide mixture of Cr_2O_3, TiO_2 and $NiCr_2O_4$, which increases the possibility of internal oxidation.

Figure 5 illustrates the surface variation of the (Ni,Pt)Al coating during isothermal oxidation at 980 °C. After 300 h oxidation, whisker-shaped oxide grains are observed on the surface, presenting the characteristics of transient oxide θ-Al_2O_3 (Figure 5a) [16–18]. The shape of oxide changes into longer whisker-like oxide after 500 h oxidation at 980 °C, as shown in Figure 5b. Figure 5c shows surface images after exposure for 1000 h, in which alumina grows continuously and gets coarser. After 1500 h, the oxide scale is still completely intact (Figure 5d), but the morphology of Al_2O_3 transforms from whisker to blade. It is found that although whisker or blade morphology appears on the outer surface after exposure for 1500 h at 980 °C, the spallation of the thin oxide scale cannot be observed and the oxide scale maintains compact and uniform, which can effectively protect the substrate alloy from oxygen invasion.

Table 1. Average composition of the regions marked in Figure 4 (EDS, at.%).

	O	Al	Ti	Cr	Ni
1	66.64	5.58	4.87	15.25	7.57
2	58.76	19.62	4.11	8.17	9.34
3	64.23	10.58	10.00	14.47	0.72
4	56.29	25.19	1.88	5.81	10.83
5	69.06	6.02	10.62	12.44	1.86
6	58.59	20.02	6.40	8.63	6.36
7	68.21	0.65	2.76	20.20	8.18
8	59.49	28.57	0.70	3.78	7.46

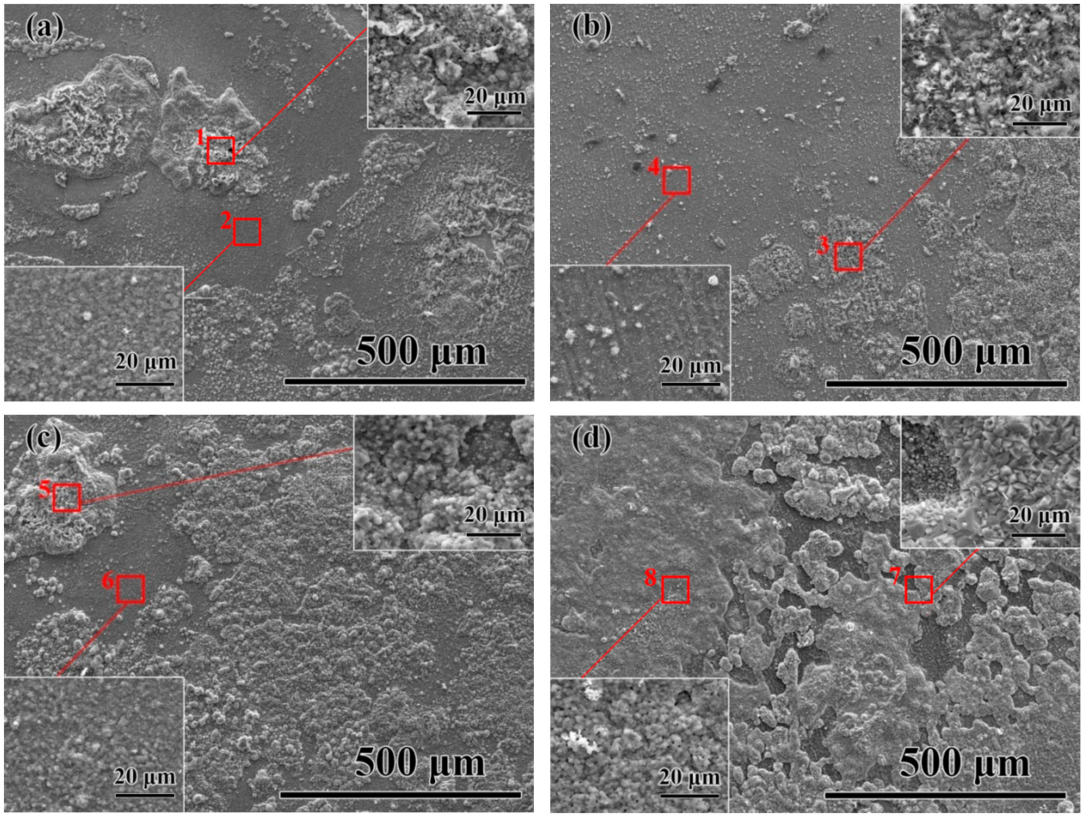

Figure 4. Surface morphologies of the SX superalloy after isothermal oxidation at 980 °C for 300 h (**a**), 500 h (**b**), 1000 h (**c**) and 1500 h (**d**).

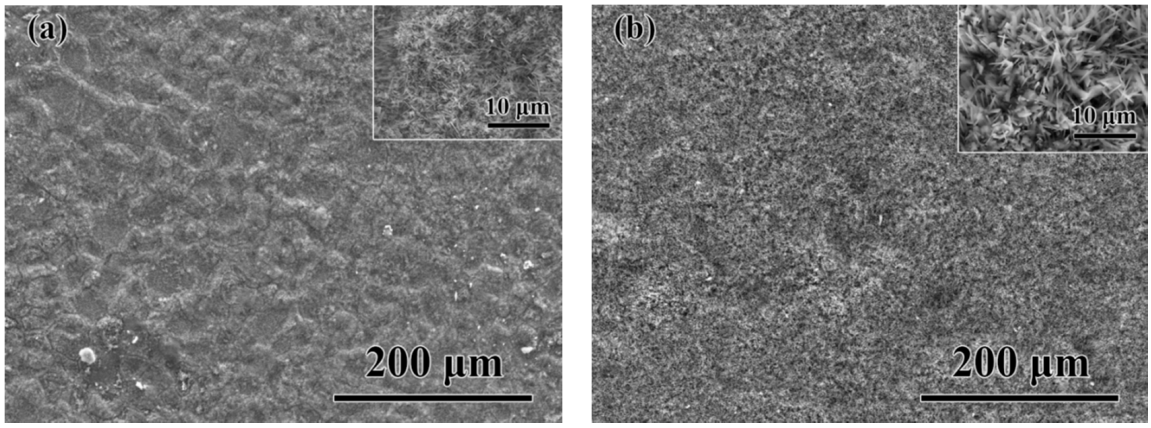

Figure 5. *Cont*.

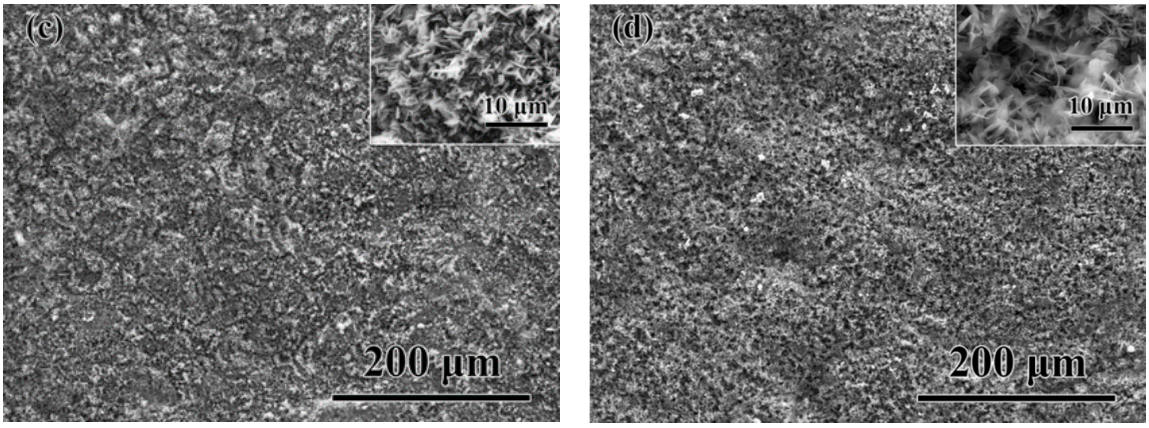

Figure 5. Surface morphologies of (Ni,Pt)Al coatings after isothermal oxidation at 980 °C for 300 h (**a**), 500 h (**b**), 1000 h (**c**) and 1500 h (**d**).

3.3. Cross-Sectional Morphology

The cross-sectional morphologies of the SX superalloy oxidized at 980 °C for different times are illustrated in Figure 6.

After oxidation for 300 h, zone A and zone B are observed obviously (Figure 6a). Zone A reveals three distinct layers, as shown clearly at high magnification in the inserted image. The combination of EDS and XRD results suggests that the outer scale comprises a mixture of Cr_2O_3, TiO_2 and a few $NiCr_2O_4$. The dense internal layer is rich in Al, showing that the Al_2O_3 layer formed. Ti-rich precipitates are visible beneath the internal layer, according to the study of Pfennig et al. [19], it is TiN. The enlarged image of zone B is shown on the right of Figure 6a, which corresponds to the cauliflower-shape region shown in Figure 4a. Along the surface to the substrate, zone B is composed of a relatively thick outer scale (mainly Cr_2O_3 + $NiCr_2O_4$ + TiO_2), white Ta-rich oxide layer (mainly Ta_2O_5) [20] close to the outer scale, internal Al_2O_3 layer and short rod-like TiN. Ti and Ta exist in the oxide layer in a unique way. Compared with zone A, zone B with relatively thick oxide scale reflects a combination of internal oxidation and external oxidation. The uneven distribution of Al in the substrate alloy plays an important role in the formation of Al_2O_3, leading to Al_2O_3 layer with different thickness.

After 500 h, from the magnified image of zone C (right of Figure 6b), it can be seen that in oxide scale a few Ta_2O_5 formed in between the loose outer layer and the internal oxide layer, followed by an oxidation-free zone with emergence of some TiN precipitates. After 1000 h, the amount of oxidation products increase with oxidation time, as shown in Figure 6c. Zone D presents a four-layer structure: The outer and internal layers remain continuous, but have been thickened with obviously loose features. When the substrate alloy was exposed for 1500 h, zone E and zone F emerged out (Figure 6). Zone E with a triple-layer structure has no difference to zone A. For the four-layer structured zone F, it can be seen that a thick and porous outer layer forms accompanied with a Ta-rich oxide product, a continuous layer of Al_2O_3 has not yet been established, and the adjacent layer is enriched with TiN (right of Figure 6d).

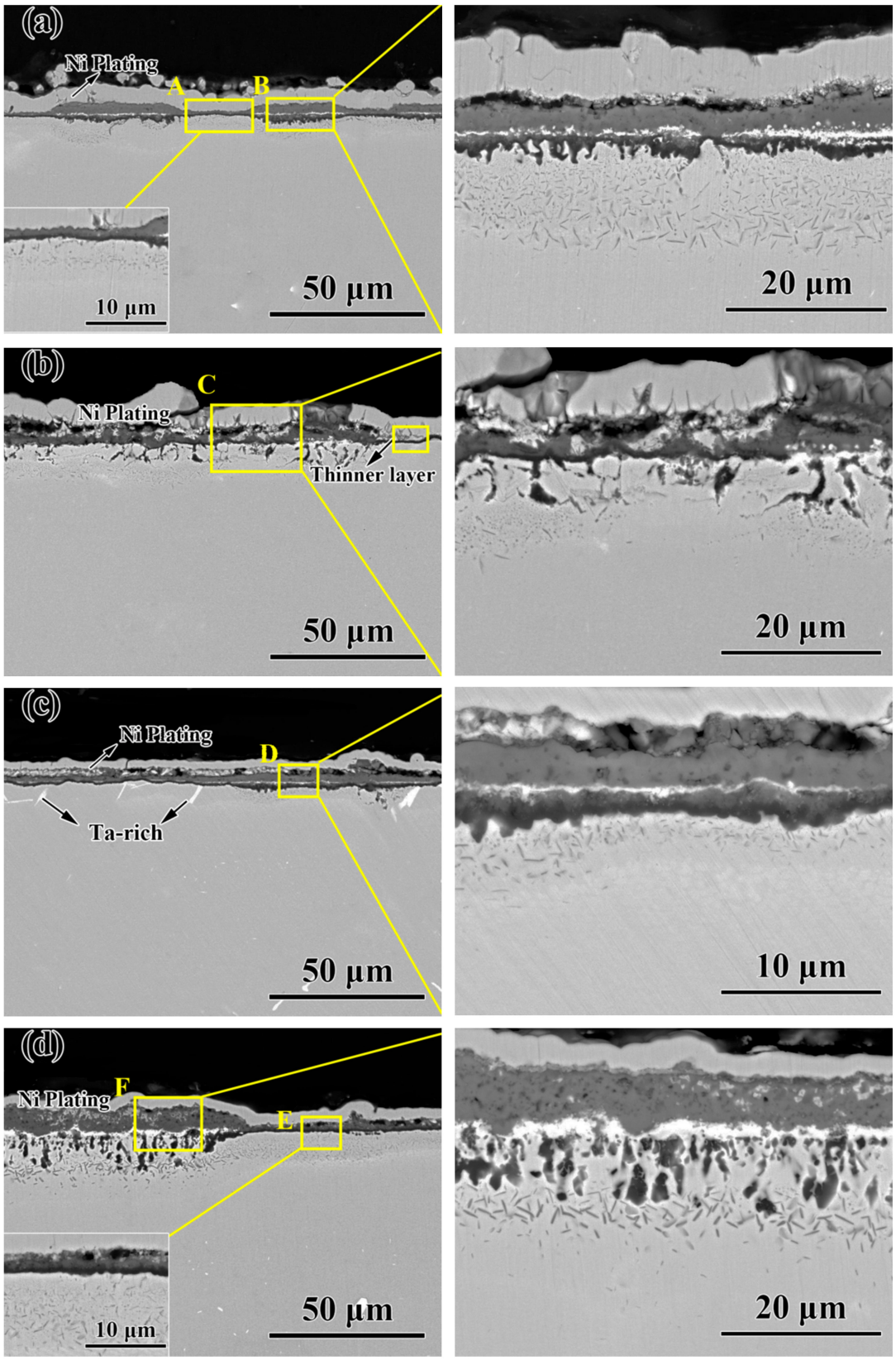

Figure 6. Cross-sectional morphologies of the SX superalloy after isothermal oxidation at 980 °C for 300 h (**a**), 500 h (**b**), 1000 h (**c**) and 1500 h (**d**) (on the right of **a**, **b**, **c** and **d** are the magnified image of **B**, **C**, **D** and **F** zones, respectively).

Figure 7 shows the cross-sectional morphologies of the (Ni,Pt)Al coatings after oxidation at 980 °C for 300, 500, 1000 and 1500 h. After 300 h, as shown in Figure 7a, the

continuous Al_2O_3 scale reveals a dual-layered structure, which is composed of a whisker-like top layer and dense internal layer, with a total thickness of ~2.1 μm. In the case of oxidation for 500 h, the oxide layer is still composed of Al_2O_3 and the total oxide scale thickness is about ~3.1 μm, as presented in Figure 7b. The average content of the coating is listed in Table 2, where the content of Al is reduced by the sustaining consumption. Meanwhile, a few β phases in the outer zone of the coating have been transformed to γ′ phases. Figure 7c shows that the oxide scale grows to the thickness of ~4.2 μm after 1000 h. The fraction of γ′ phase gets increased slightly in the outer zone. As the oxidation time prolonged to 1500 h, there is neither a significant change of the morphology nor of the composition of the oxide scale. A continuous Al_2O_3 scale has formed with no cracking or void formation (Figure 7d) and the scale thickness increases to ~5 μm. The Al-rich β phase in the outer zone is gradually converted to the γ′ phase due to Al depletion induced by oxidation. However, the degradation rate from β to γ′ is slow, which is able to form a compact Al_2O_3 scale for future long term. It is confirmed that the (Ni,Pt)Al coating can efficiently protect the substrate from aggressive oxidation attack.

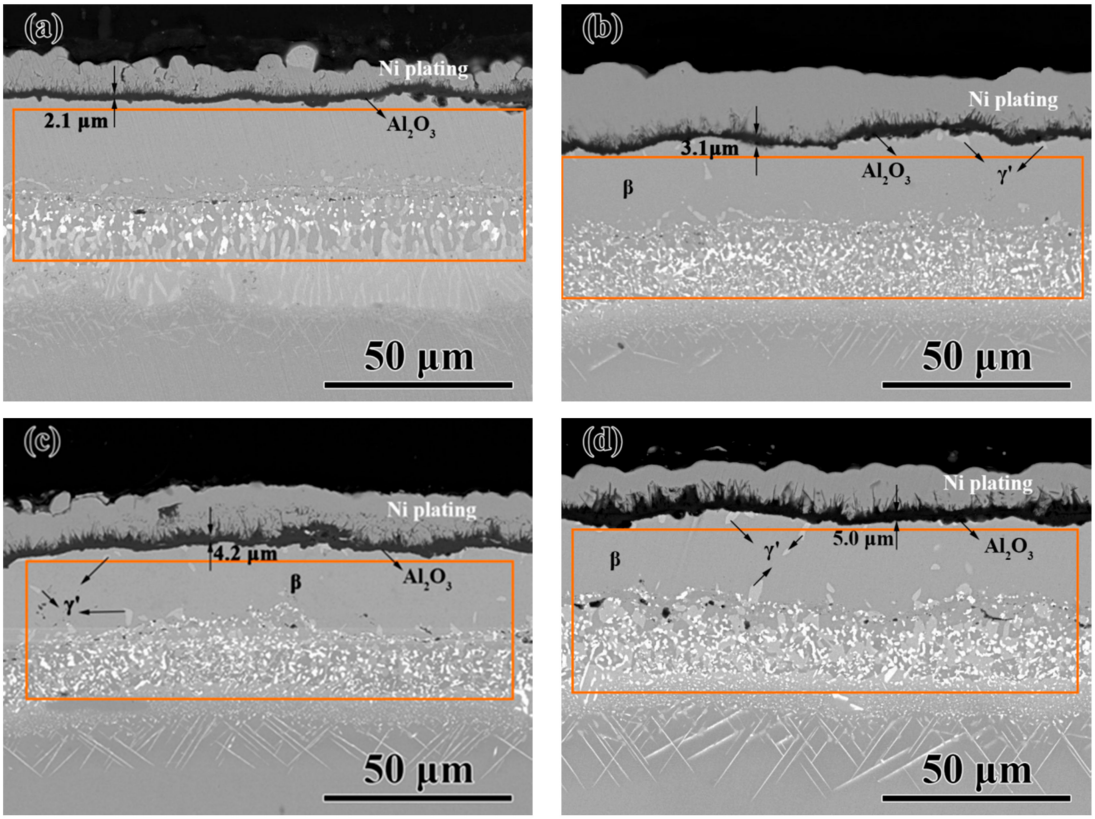

Figure 7. Cross-sectional morphologies of (Ni,Pt)Al coating after isothermal oxidation at 980 °C for 300 h (**a**), 500 h (**b**), 1000 h (**c**) and 1500 h (**d**).

Table 2. Average contents of the marked regions of (Ni,Pt)Al coating after isothermal oxidation at 980 °C for different times, showing the main elements of Ni, Pt and Al (at.%).

Oxidation Time	Pt	Ni	Al
300 h	3.45	54.42	**42.13**
500 h	3.87	56.63	**39.50**
1000 h	3.11	58.62	**38.27**
1500 h	4.14	59.59	**36.27**

4. Discussion

4.1. Oxidation Behavior of SX Superalloy at 980 °C

When the oxygen partial pressure pO_2 on the metal surface is higher than the equilibrium value of pO_2, the metal oxidation reaction will occur:

$$M + O_2 = MO_2 \quad (1)$$

Following this reaction for M/MO_2 the equilibrium value of pO_2 is given by,

$$pO_2 = \exp \int \left(\frac{\Delta G^{\theta}_{MO2}}{RT}\right) \quad (2)$$

According to Wagner's theory [21], the critical content N_B in the alloy for the formation of external oxide scale can be expressed as following:

$$N_B > \left[\frac{\pi g^*}{2b} \cdot N_O \frac{D_O \cdot V_m}{D_B \cdot V_{OX}}\right]^{1/2} \quad (3)$$

where π and g* (close to ~0.3) are constants, N_oD_o is the diffusion coefficient for oxygen in alloy, V_m is the molar volume of metal, D_B is the diffusivity of species B, and V_{ox} is the molar volume of oxides.

Combining surface and cross sectional morphologies together, the oxidation procedure of the SX superalloy at 980 °C can be illustrated, as in Figure 8. The inhomogeneity of the structure and composition for the substrate alloy promotes the production of the complex oxides during oxidation, which is responsible for the varied oxide microstructure at surface. At the initial stage of oxidation, the concentration of Cr and Ti in SX alloy is greater than their critical content N_B to generate a continuous outer layer dominated by Cr_2O_3 + $NiCr_2O_4$ + TiO_2. Nevertheless, the concentration of the Al content is below its critical value required for forming external $A1_2O_3$ scale. The pO_2 is reduced beneath the outer oxide, which enhances the selective growth of Al_2O_3 below the non-protective outer oxide mixture of Cr_2O_3 + $NiCr_2O_4$ and TiO_2, leading to the lateral growth and coalescence of the Al_2O_3 precipitates. After a period of oxidation, a continuous Al_2O_3 internal layer has already formed, as shown in Figure 8a.

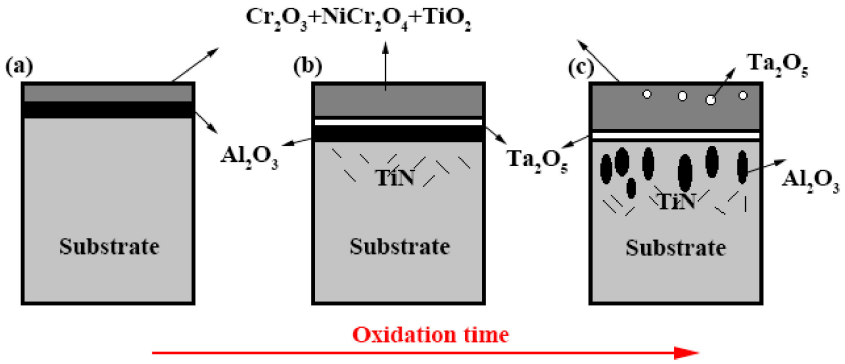

Figure 8. Schematic diagram shows the oxidation process of substrate alloy at 980 °C.

As the oxidation time increases, the content of Al in local substrate is reduced by spallation of oxide scale, leading to incapability of supplying Al required to maintain a continuous internal Al_2O_3 scale. This allows the outward diffusion of Cr, Ti, Ni and Ta, and the inward diffusion of nitrogen and oxygen, which cause the phenomenon that the non-protective outer layer grows and Ta_2O_5 embeds between the outer layer and internal layer. Furthermore, the aggravation of internal oxidation degree and formation of TiN can be observed (Figure 8b). This process is thermodynamically feasible, because the Gibbs free energy of TiN is more negative than that of AlN, and also Al has been depleted

underneath the outer layer in the alloy due to the internal oxidation. As a result, more thermodynamically stable TiN formed instead of AlN. With further oxidation, the thickness of porous non-protective oxide layer increases, and Ta_2O_5 dispersed and approached to the surface due to outward diffusion of Ta and the growth of outer layer. Moreover, the regions of internal oxidation and TiN both expanded, as shown in Figure 8c. In conclusion, the oxide product formed on the surface of bare SX superalloy cannot prevent the substrate from oxidation invasion.

4.2. Oxidation Behavior of (Ni,Pt)Al Coating at 980 °C

The results have demonstrated that better oxidation performance is observed on SX specimens deposited with (Ni,Pt)Al coating than the substrate alloy. The protection against high-temperature oxidation is provided by the (Ni,Pt)Al coating, which relies on the formation of a continuous Al_2O_3 scale on the surface. The Al-rich β-NiAl phase enhances the selective growth of thermodynamically stable Al_2O_3. Normally, the effective diffusion rates of oxygen and metal ions through Al_2O_3 scale are relatively low, which retards the growth rate of the oxide scale [22]. With addition of Pt, it is not prone to cracking and spalling of alumina scale. [1,2,23,24]. The oxide scale thickness as a function of oxidation time for the samples that coated with (Ni,Pt)Al are shown in Figure 9, where the kinetic curve basically follows a parabolic law. It can be seen from Figure 7 that the Al-rich β phase gradually transformed into the Al-poor γ′ phase due to Al diffusion and depletion [7]. Generally, Al in the (Ni,Pt)Al coating is consumed gradually over time, which acts as one of the reasons for the eventual failure of the coating [21]. However, during isothermal oxidation at 980 °C for 1500 h, the (Ni,Pt)Al coating has shown relatively slow degradation rate and sufficient Al concentration to ensure the compact and self-healing formation of exclusive Al_2O_3 scale.

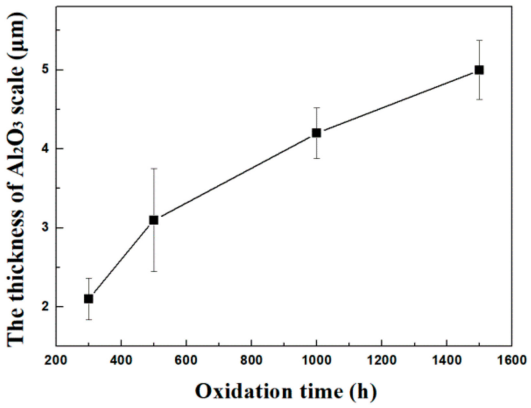

Figure 9. The relationship between the thickness of Al_2O_3 scale of the (Ni,Pt)Al coating via isothermal oxidation time at 980 °C.

Figure 7 shows the Al_2O_3 scale is dual-layered with a whisker-like top layer followed by a dense internal layer. It is reported [25] that, in stress-free condition, α-Al_2O_3 produces luminescence peaks located at 14,402 and 14,432 cm^{-1}, and θ-Al_2O_3 located at 14,575 and 14,645 cm^{-1}. Figure 10 shows the luminescence spectra of the Al_2O_3 scale formed on the (Ni,Pt)Al coating. Both θ-Al_2O_3 phase and α-Al_2O_3 phase co-existed from 300 h to 1500 h oxidation at 980 °C. As suggested by Young et al. [16], at 980 °C the oxide scale with existence of θ-Al_2O_3 is formed on the surface of NiAl coating. At the initial oxidation stage, whisker-like θ-Al_2O_3 grains grew outwardly from the original coating surface and covered the surface rapidly. However, α-Al_2O_3 grains only formed beneath the outer θ-Al_2O_3 grains and then grew into a dense and continuous layer [17,26], which is consistent with the structure of the surface scale formed on the NiAl coating, as shown in Figure 7. Generally, the growth of θ-Al_2O_3 is predominantly controlled by the outward diffusion of Al, in which the fast growth requires massive transport of Al. The θ-Al_2O_3 contains

a high amount of defects, causing the outward diffusion of Al through the whiskers to the outer surface possible. At the same time, a small amount of θ-Al_2O_3 is transformed to α-Al_2O_3. However, the morphologies of α-Al_2O_3 still retained whisker- or blade-like oxides after this transformation [25,26]. Therefore, the outer layer probably also contains a certain amount of α-Al_2O_3 phase in addition to θ-Al_2O_3 phase.

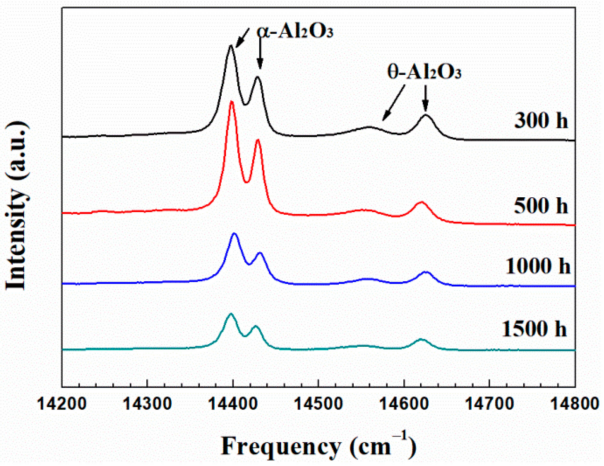

Figure 10. Luminescence spectra of the (Ni,Pt)Al coating oxidized at 980 °C at different times.

During the initial oxidation period and at lower temperature (such as 800 °C), metastable alumina oxide series grow, such as γ-, δ- and θ-Al_2O_3 [27]. Brumm et al. [28] found that the transformation from θ-Al_2O_3 to α-Al_2O_3 could be observed in the temperature range 950–1050 °C. Normally, α-Al_2O_3 grows by both outward diffusion of aluminum and inward diffusion of oxygen, whereas θ-Al_2O_3 grows mainly by outward diffusion of aluminum reacting with oxygen at the upmost surface [29,30]. The θ-Al_2O_3 that transforms to α-Al_2O_3 varies significantly under different experimental conditions. Either addition of elements, oxidation temperature and even environment would play a role in influencing metastable θ-Al_2O_3 growth and transformation [31]. Cr in the β-NiAl coating can accelerate the transformation from θ-Al_2O_3 to α-Al_2O_3, because the initial formation of Cr_2O_3 increases nuclei sites for α-Al_2O_3 formation. The addition of larger ions of Y or Zr inhibits the outward transport of Al, which tends to delay θ-Al_2O_3 to α-Al_2O_3 transition. At higher temperature, the metastable alumina phases are just present for a short time, while they exist for a long-term at lower temperature. In the present study, the moderate-high temperature of 980 °C permits the existence of θ-Al_2O_3 till 1500 h (see Figure 10).

Numerous studies have reported that the addition of Pt can significantly increase the adhesion of the oxide scale, improve oxidation performance and prolong the service life of the alloy at elevated temperatures. Once oxidized at even higher temperature (over 1100 °C), whisker- or blade-like θ-Al_2O_3 were not observed for the Pt-modified aluminide coating due to the extremely short transformation time that cannot be perceived [28–33]. Chen et al. [32] reported that a combination process of nano-powder mixing and SPS approach was used to produce a Pt-modified β-NiAl coating, in which Pt may favor the θ-to-α transformation, but the main contributing factor should be given to the higher oxidation temperature of 1150 °C. Liu et al. [34] concluded that Pt addition in γ-Ni/γ′-Ni_3Al coatings can slow down the θ-Al_2O_3 to α-Al_2O_3 transformation and thus extend the metastable θ-Al_2O_3 duration. Wit [33] et al. found that the oxide scale on the PtNiAl sample is grown mainly by aluminum transport at 900 °C. The θ-Al_2O_3 with needle and blade structure formed on top of a compact layer, which still existed after 50 h at 1000 °C. The more Pt addition results in more θ-Al_2O_3 in the oxide scale [34].

The presence of a large amount of Pt in β-NiAl will change the oxidation mechanism. On one hand, Pt can hinder the diffusion of oxygen through oxide scale, whereas promote the diffusion of Al. On the other hand, high content of Al is unfavorable with growth of

α-Al_2O_3. A metastable θ-Al_2O_3 grows mainly through the outward diffusion of Al and it contains a high amount of defects promoting Al diffusion through the oxide to the outer surface conveniently, which will lead to a continuous growth of θ-Al_2O_3. Furthermore, the moderate-high temperature retards θ-to-α transformation, resulting in long-term existence of metastable θ alumina particles. In addition, orientation plays part of a role in θ-Al_2O_3 to α-Al_2O_3 transformation as well [35]. The θ-Al_2O_3 was retained in the oxide scale after 1500 h at 980 °C, as shown in Figure 10, which showed an effect of delaying θ-to-α Al_2O_3 phase transformation. This seems to be disadvantageous to the scale spallation resistance. However, after long term oxidation, the oxide scale still keeps intact and dense (Figure 7). The addition of Pt can significantly improve spallation resistance of the oxide scale and, consequently, contribute to the superior protection for long-term oxidation. That is to say, the dual-layer structure of alumina scale applied no deterioration to the oxidation resistance at all, which derived from the ability of forming exclusively pure alumina scale.

5. Conclusions

The microstructural evolution and isothermal oxidation behavior of Pt-modified aluminide coatings were investigated at 980 °C in static air in comparison with bare SX superalloy. The following conclusions can be drawn from the above experimental results:

- Building of layered oxide on SX superalloy changed constantly. The multi-layered scale mainly consisted of a thick and porous outer layer, which was composed of the non-protective oxide mixture of Cr_2O_3 + $NiCr_2O_4$ + TiO_2, and an internal layer of Al_2O_3. As the oxidation time prolonged, the thickness of the loose outer layer increased and the internal alumina scale became discontinuous, which allowed the inward diffusion of nitrogen and oxygen to form Ta_2O_5 and TiN, resulting in the aggravation of internal oxidation.
- During oxidation, a continuous Al_2O_3 scale formed on the surface of the Pt-modified aluminide coating, which held a dual-layer structure with a whisker/blade-like outer layer and a dense internal layer. The long-term existence of θ-Al_2O_3 whiskers was attributed to the moderate-high temperatures and the addition of Pt. The Pt-modified aluminide coating confirmed its competence in service of a relatively long lifetime.
- In the oxidation process, the β-phase in the outer zone of the Pt-modified aluminide coating gradually converted to the γ' phase due to aluminum depletion induced by oxidation.
- In short, the Pt-modified aluminide coating showed the best oxidation resistance by forming a continuous Al_2O_3 scale and possessing a slow degradation rate from β to γ'. It can be used for protecting the hot components of electric gas turbines, small type turbine engines and turboshaft engines.

Author Contributions: Writing—original draft preparation, methodology, investigation, Y.L.; data curation, S.L.; conceptualization, resource, C.Z.; writing—review and editing, funding acquisition, Z.B.; supervision, N.X., Z.B. All authors have read and agreed to the published version of the manuscript.

Funding: This research was funded by the R & D Program in Key Fields of Guangdong Province (2019B010936001). This work was also supported by National Engineering Laboratory for Marine and Ocean Engineering Power System—Laboratory for Ocean Engineering Gas Turbine.

Institutional Review Board Statement: Not applicable.

Informed Consent Statement: Not applicable.

Data Availability Statement: The raw/processed data required to reproduce these findings cannot be shared at this time as the data also forms part of an ongoing study.

Conflicts of Interest: The authors declare no conflict of interest. The funders had no role in the design of the study; in the collection, analyses, or interpretation of data; in the writing of the manuscript, or in the decision to publish the result.

References

1. Jiang, C.Y.; Yang, Y.F.; Zhang, Z.Y.; Bao, Z.B.; Chen, M.H.; Zhu, S.L.; Wang, F.H. A Zr–doped single–phase Pt–modified aluminide coating and the enhanced hot corrosion resistance. *Corros. Sci.* **2018**, *133*, 406–416. [CrossRef]
2. Liu, G.; Niu, Y.; Wang, W. Oxidation behaviour of aluminide and Pt–modified aluminide coatings on CMSX–4 at 1100 °C. *Corros. Sci. Technol. Prot.* **2001**, *13*, 400–404.
3. Meng, X.X.; Yuwen, P.; Shao, W.; Qu, W.T.; Zhou, C.G. Cyclic oxidation behaviour of Co/Si co–doped β–NiAl coating on nickel based superalloys. *Corros. Sci.* **2018**, *133*, 112–119. [CrossRef]
4. Liu, H.; Li, S.; Jiang, C.Y.; Yu, C.T.; Bao, Z.B.; Zhu, S.L.; Wang, F.H. Preparation and oxidation performance of a low–diffusion Pt–modified aluminide coating with Re–base diffusion barrier. *Corros. Sci.* **2020**, *168*, 108582. [CrossRef]
5. Rafiee, H.; Arabi, H.; Rastegari, S. Effects of temperature and Al–concentration on formation mechanism of an aluminide coating applied on superalloy IN738LC through a single step low activity gas diffusion process. *J. Alloys Compd.* **2010**, *505*, 206–212. [CrossRef]
6. Li, M.F.; Kong, C.; Zhang, J.Q.; Zhou, C.G.; Young, D.J. Oxidation behavior of Ni–Al coating with and without a Ni–Re diffusion barrier in dry CO_2 gas at 650 °C. *Corros. Sci.* **2019**, *149*, 236–243. [CrossRef]
7. Yang, Y.F.; Jiang, C.Y.; Zhang, Z.Y.; Bao, Z.B.; Chen, M.H.; Zhu, S.L.; Wang, F.H. Hot corrosion behaviour of single–phase platinum–modified aluminide coatings: Effect of Pt content and pre–oxidation. *Corros. Sci.* **2017**, *127*, 82–90. [CrossRef]
8. Zhou, Y.H.; Zhao, X.F.; Zhao, C.S.; Hao, W.; Wang, X.; Xiao, P. The oxidation performance for Zr–doped nickel aluminide coating by composite electrodepositing and pack cementation. *Corros. Sci.* **2017**, *123*, 103–115. [CrossRef]
9. Zhang, C.Y.; Ma, Z.; Dong, S.Z.; Xu, M.M.; Li, S.; Zhang, C.; Jiang, C.Y.; Bao, Z.B.; Zhu, S.L.; Wang, F.H. High-temperature oxidation behaviour of refurbished (Ni,Pt)Al coating on Ni-based superalloy at 1100 °C. *Corros. Sci.* **2021**, *187*, 109521. [CrossRef]
10. Yang, Y.F.; Jiang, C.Y.; Yao, H.R.; Bao, Z.B.; Zhu, S.L.; Wang, F.H. Preparation and enhanced oxidation performance of a Hf-doped single-phase Pt-modified aluminide coating. *Corros. Sci.* **2016**, *113*, 17–25. [CrossRef]
11. Yang, Y.F.; Jiang, C.Y.; Bao, Z.B.; Zhu, S.L.; Wang, F.H. Effect of aluminisation characteristics on the microstructure of single phase β-(Ni,Pt)Al coating and the isothermal oxidation behavior. *Corros. Sci.* **2016**, *106*, 43–54. [CrossRef]
12. Swadźba, R.; Hetmańczyk, M.; Sozańska, M.; Witala, B.; Swadźba, L. Structure and cyclic oxidation resistance of Pt, Pt/Pd-modified and simple aluminide coatings on CMSX-4 superalloy. *Surf. Coat. Technol.* **2011**, *206*, 1538–1544. [CrossRef]
13. Swadźba, R.; Hetmańczyk, M.; Wiedermann, J.; Swadźba, L.; Moskal, G.; Witala, B.; Radwański, K. Microstructure degradation of simple, Pt- and Pt+Pd-modified aluminide coatings on CMSX-4 superalloy under cyclic oxidation conditions. *Surf. Coat. Technol.* **2013**, *215*, 16–23. [CrossRef]
14. Yu, C.T.; Liu, H.; Ullaha, A.; Bao, Z.B.; Zhu, S.L.; Wang, F.H. High–temperature performance of (Ni,Pt)Al coatings on second–generation Ni–base single–crystal superalloy at 1100 °C: Effect of excess S impurities. *Corros. Sci.* **2019**, *159*, 108115. [CrossRef]
15. Liu, H.; Xu, M.M.; Li, S.; Bao, Z.B.; Zhu, S.L.; Wang, F.H. Improving cyclic oxidation resistance of Ni_3Al-based single crystal superalloy with low-diffusion platinum-modified aluminide coating. *J. Mater. Sci. Technol.* **2020**, *54*, 132–143. [CrossRef]
16. Young, D.J. High Temperature Oxidation and Corrosion of Metals. *Corros. Ser.* **2008**, *1*, 219–226.
17. Alvarado–Orozco, J.M.; Morales–Estrella, R.; Boldrick, M.S.; Ortiz–Merino, J.L.; Konitzer, D.G.; Trápaga–Martínez, G.; Muñoz–Saldaña, J. First Stages of Oxidation of Pt–Modified Nickel Aluminide Bond Coat Systems at Low Oxygen Partial Pressure. *Oxid. Met.* **2012**, *78*, 269–284. [CrossRef]
18. An, T.F.; Guan, H.R.; Sun, X.F.; Hu, Z.Q. Effect of the θ–α–Al_2O_3 Transformation in Scales on the Oxidation Behavior of a Nickel–Base Superalloy with an Aluminide Diffusion Coating. *Oxid. Met.* **2000**, *54*, 301–316. [CrossRef]
19. Pfennig, A.; Fedelich, B. Oxidation of single crystal PWA 1483 at 950 °C in flowing air. *Corros. Sci.* **2008**, *50*, 2484–2492. [CrossRef]
20. Yang, L.L.; Chen, M.H.; Wang, J.L.; Bao, Z.B.; Zhu, S.L.; Wang, F.H. Oxidation of duplex coatings with different thickness ratio of the internal nanocrystalline layer to the outer NiCrAlY one. *Corros. Sci.* **2018**, *143*, 136–147. [CrossRef]
21. Lou, H.; Zhu, S.; Wang, F. Rehealing ability of oxide scales formed on microcrystalline K38G coatings. *Oxid. Met.* **1995**, *43*, 317–328. [CrossRef]
22. Zhao, C.S.; Zhou, Y.H.; Zou, Z.H.; Luo, L.R.; Zhao, X.F.; Guo, F.W.; Xiao, P. Effect of alloyed Lu, Hf and Cr on the oxidation and spallation behavior of NiAl. *J. Corros. Sci.* **2017**, *126*, 334–343. [CrossRef]
23. Oskay, C.; Galetz, M.C.; Murakami, H. Oxide scale formation and microstructural degradation of conventional, Pt–and Pt/Ir–modified NiAl diffusion coatings during thermocyclic exposure at 1100 °C. *Corros. Sci.* **2018**, *144*, 313–327. [CrossRef]
24. Liu, G.; Niu, Y.; Wang, W.; Wu, W.T. Oxidation behaviour of Pt–modified aluminide coatings on IN738 at 1100 °C. *J. Chin. Soc. For. Corros. Prot.* **2001**, *01*, 55–59.
25. Yan, K.; Guo, H.B.; Gong, S.K. High–temperature oxidation behavior of minor Hf doped NiAl allo in dry and humid atmospheres. *Corros. Sci.* **2013**, *75*, 337–344. [CrossRef]
26. Hou, P.Y.; Paulikas, A.P.; Veal, B.W. Stress development and relaxation in Al_2O_3 during early stage oxidation of β–NiAl. *Mater. High. Temp.* **2005**, *22*, 535–543. [CrossRef]
27. Svensson, H.; Angenete, J.; Stiller, K. Microstructure of oxide scales on aluminide diffusion coatings after short time oxidation at 1050 °C. *Surf. Coat. Technol.* **2004**, *177*, 152–157. [CrossRef]
28. Brumm, M.W.; Grabke, H.J. The oxidation behavior of NiAl—I. Phase transformations in the alumina scale during oxidation of NiAl and NiAl–Cr alloys. *Corros. Sci.* **1992**, *33*, 1667–1690. [CrossRef]

29. Liu, G.M.; Li, M.S.; Zhu, M.; Zhou, Y.C. Transient of alumina oxide scale on β–NiAl coated on M38G alloy at 950 °C. *Intermetallics* **2007**, *15*, 1285–1290. [CrossRef]
30. Pint, B.A.; Martin, J.R.; Hobbs, L.W. The oxidation mechanism of θ–Al_2O_3 scales. *Solid State Ion.* **1995**, *78*, 99–107. [CrossRef]
31. Chen, C.F.; Rühle, M. Transient alumina transformation on a sputtered K38G nanocrystalline coating. *Surf. Coat. Technol.* **2005**, *191*, 263–266. [CrossRef]
32. Chen, W.F.; Shan, X.J.; Li, H.; Guo, Y.; Guo, F.W.; Zhao, X.F.; Ni, N.; Xiao, P. Effects of iron and platinum on the isothermal oxidation of β–NiAl overlay coatings fabricated by spark plasma sintering. *Surf. Coat. Technol.* **2019**, *382*, 125178. [CrossRef]
33. De Wit, J.; Van Manen, P. The precious metal effect in high temperature corrosion. *Mater. Sci. Forum* **1994**, *154*, 109–118. [CrossRef]
34. Liu, C.; Chen, Y.; Eggeman, A.S.; Brewster, G.; Xiao, P. Pt effect on early stage oxidation behaviour of Pt–diffused γ–Ni/γ′–Ni_3Al coatings. *Acta Mater.* **2020**, *189*, 232–247. [CrossRef]
35. Grabke, H.J. Oxidation of NiAl and FeAl. *Intermetallics* **1999**, *7*, 1153–1158. [CrossRef]